Ultra-short optical pulse generation in micro OLEDs and the perspective of lasing

Document status and date:
Published: 01/03/2022

Document Version:
Publisher's PDF, also known as Version of Record (includes final page, issue and volume numbers)

Please check the document version of this publication:

• A submitted manuscript is the version of the article upon submission and before peer-review. There can be important differences between the submitted version and the official published version of record. People interested in the research are advised to contact the author for the final version of the publication, or visit the DOI to the publisher's website.
• The final author version and the galley proof are versions of the publication after peer review.
• The final published version features the final layout of the paper including the volume, issue and page numbers.

Link to publication

Ultra-short optical pulse generation in micro OLEDs and the perspective of lasing

To cite this article: Daan Lenstra *et al* 2022 *J. Opt.* **24** 034007

View the article online for updates and enhancements.

Ultra-short optical pulse generation in micro OLEDs and the perspective of lasing

Daan Lenstra[1,*] , **Alexis P A Fischer**[2,3] , **Amani Ouirimi**[2,3],
Alex Chamberlain Chime[2,3,4] , **Nixson Loganathan**[2,3] **and Mahmoud Chakaroun**[2,3]

[1] Institute of Photonics Integration, Eindhoven University of Technology, P.O. Box 513, 5600MB Eindhoven, The Netherlands
[2] Université Sorbonne Paris Nord, Laboratoire de Physique des Lasers, UMR CNRS 7538, 99 avenue JB Clement, Villetaneuse-F, 93430, France
[3] Université Sorbonne Paris Nord, Centrale de Proximite en Nanotechnologies de Paris Nord, 99 Avenue JB Clement, Villetaneuse-F, 93430, France
[4] IUT-FV de Bandjoun, Université de Dschang, BP 134 Bandjoun, Cameroun

E-mail: dlenstra@tue.nl

CrossMark

Abstract

We report experimental and theoretical investigations with an in-house fabricated tris(8-hydroxyquinoline)-aluminum (Alq3)-based high-speed micro-organic light-emitting diodes (μ-OLEDs) and demonstrate very promising optical pulse responses as short as 400 ps. With a model for an electrically pumped OLED, we simulate the emission of sub-nanosecond optical pulses. The model includes field-dependent (Poole-Frenkel) Langevin recombination and reabsorption of photons by singlets (Stokes-shifted), and by triplets (TA). The good agreement between the measurement and the simulation is the basis for further study of the prospects on the ps time scale, i.e. stimulated emission and conditions for laser operation. For an Alq3-based micro-OLED with high-Q optical cavity, we predict pulsed laser operation with damped relaxation oscillations in the GHz regime and several orders of magnitude linewidth narrowing, but only during 3 ns at most. The simulated current density threshold values vary from 10 kA cm^{-2} for $Q = 500$ to less than 1 kA cm^{-2} for $Q = 1000$. No continuous-wave (CW) lasing is found due to the accumulation of triplet excitons for $t > 5$ ns, which has two deteriorating effects, (a) suppression of the gain-providing singlet excitons due to singlet-triplet absorption and (b) suppression of the photon density due to photon absorption by triplets (TA). Prospects for CW-lasing with other organic molecules are discussed.

Keywords: optoelectronics, OLED, laser, organic diode laser, laser dynamics

(Some figures may appear in colour only in the online journal)

* Author to whom any correspondence should be addressed.

1. Introduction

To confirm that a future of organic optoelectronics could be 'far beyond display and lighting' applications, we present results of a study of micro-organic light-emitting diode (μ-OLED) devices under nanosecond and sub-nanosecond electrical pulse excitation. The results strongly confirm the promise of a scientific and technological revolution with the ultra-fast dynamics of organic optoelectronics and laser operation, exceeding state-of-the-art results for GaN μ-LEDs and OLEDs [1, 2].

An OLED operates on the spontaneous emission of light from an organic molecular material. In this material, optically active excitons are created by recombination of polarons, where the latter are formed under the influence of an applied electrical potential between two electrodes. If both the density of emitting excitons and emitted photons can be kept sufficiently large, stimulated emission can provide the optical gain necessary for laser operation. This can be achieved by placing the emitting region in an optical cavity with high quality factor to keep the photons in the gain region during a sufficiently long time. This forms the basis for an organic diode laser (ODL) with anticipated applications in spectroscopy, sensing, environmental monitoring, optical communication, and short-haul data transfer [1–3].

Since the demonstration of 'plastic' conductivity by Heeger in 1977 [4], organic semiconductor technology has developed into an active research field for, among others, organic photovoltaic cells [5, 6], organic field-effect transistors [7] and OLEDs [8]. It is generally thought that OLEDs are typically slow as far as their modulation capacity concerns [9]. In fact, OLEDs have low bandwidth which is mainly due to their capacitance-like behavior [9]. Its planar structure of some few hundreds of nanometers thickness forms a high capacitance which drastically limits the bandwidth and consequently the modulation rate. In some few recent works, small size OLEDs have been considered as organic light source emitter for short-range plastic optical fibers or wireless free space optical link ensuring transmission rate exceeding 1 Gb s−1 with 245 MHz bandwidth [2, 10]. These promising results are of the same order of magnitude in terms of bandwidth as GaN microLEDs, despite their relative larger active area compared to their inorganic counterparts, and this is the proof that they are serious alternatives. Recent advances in terms of response time in our team [11] suggest very high-speed response possibilities as already predicted by Braun *et al* [12].

Our team has shown that sub-nanosecond electrical pulses can be applied to OLEDs by reducing their active area to $\leq 10^{-4}\,\text{cm}^2$ and by using coplanar wave-guided (CPW) electrode [11]. Here we have used this technology to successfully excite 400 ps to 1 ns electrical pulses and observe for Alq3 equally short generated optical pulses. With a model based on four rate equations for an electrically pumped OLED, we simulate the generation of these sub-nano second optical pulses. This model is an improved version derived from an earlier published model [13] including Stoke-shifted reabsorption and field-dependent (Poole-Frenkel) Langevin recombination. The
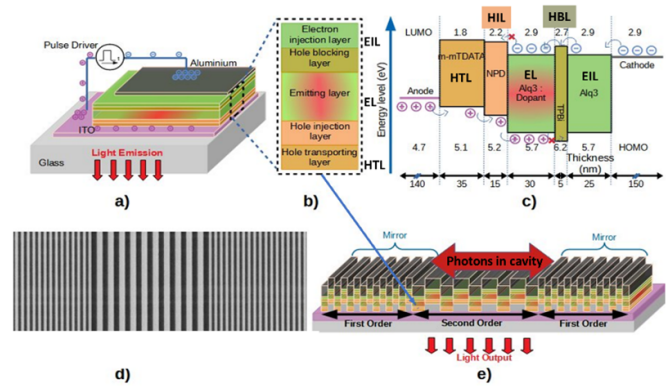
Figure 1. Schematics and direction of light emission of an ODL. In (a) and (b) the layer structure in one basic unit is indicated and in (c) the corresponding energy level diagram. In (d) a top view photograph shows the second-order grating sandwiched between the two first-order gratings and (e) presents a sketch of the ODL structure indicating the confined light between the mirrors formed by the first-order gratings. The blue arrow starting from (b) points to one of the various units in (e) that provide the optical gain in the cavity formed by the grating structure. Reproduced from [13]. CC BY 4.0.

results yield good agreement with the above-mentioned measurements.

This establishes a basis for further study of the predictions for ultra-short dynamics on the ps time scale, i.e. stimulated emission and conditions for laser operation. For an OLED that can be integrated with a high-Q cavity, for instance by utilizing gratings for light confinement and outcoupling, we predict laser operation characterized by damped relaxation oscillations in the GHz regime and several orders of magnitude linewidth narrowing.

Organic lasers can profit from a nearly unlimited availability of electroluminescent organic materials [14], each of which with special properties and covering continuously the ultraviolet, visible, and infrared spectrum. Nearly all reported solid-state organic lasers are realized by *optical pumping* of OLEDs with integrated optical cavity [15–17]. In case of *electrical injection*, gain quenching due to the accumulation of triplet excitons is considered to prevent laser oscillations build up by stimulated emission. One noteworthy exception is the modest claim of an indication for lasing in an electrically pumped organic diode by Sandanayaka *et al* [18] with the organic material BsB-Cz in an OLED configuration like the sketch in figure 1.

In this paper, we will present an improved version of our rate-equation theory for an *electrically injected* ODL [13, 19], present simulation results for operation below and above laser threshold and discuss prospects for steady-state laser operation.

2. Characterization of the ODL

An ODL is an OLED integrated with an optical cavity. The layer structure of the organic heterostructure in one basic unit

of the OLED is sketched in figures 1(a)–(c). These units are integrated with the grating structure shown in figure 1(d), which consists of a second-order Bragg grating sandwiched between two first-order Distributed Bragg Reflector (DBR) gratings. The latter form the mirrors (in the planar direction) whereas the former provides the vertical outcoupling of the light captured in the cavity structure (see figure 1(e)). The schematic energy level diagram corresponding to figure 1(a) is depicted in figure 1(c). The blue arrow from figure 1(b) points to one of the various organic heterostructure units in figure 1(e). All together, they deliver the optical gain in the cavity formed by the grating structure.

Due to the applied voltage, electron-like (i.e. negatively charged) polarons and hole-like (positively charged) polarons are created in the regions indicated electron injection layer and hole transport layer (HTL), respectively, in figure 1(b). Both types of polarons diffuse to the emitting layer (EL, see figure 1(c)), where the hole-injection layer (HIL) prevents the electron-like polarons from passing and the hole-blocking layer (HBL) blocks the hole-like polarons. In this way, both types of polarons accumulate in EL, where they recombine and form excitons, 25% singlet and 75% triplet excitons [20]. Due to selection rules, the singlet excitons can emit light by decaying to the ground state; the decay of a triplet exciton to the ground state is optically forbidden.

The singlet excitons in the EL are the source of the optical gain. After emission of a photon, whether spontaneously or by stimulated emission, the singlet exciton disappears, leaving the molecule in the ground state. Several other, non-radiative, decay channels exist for the singlet excitons, notably intersystem crossing (ISC), singlet-singlet annihilation (SSA), singlet-triplet annihilation (STA) and singlet-polaron annihilation (SPA). These decay processes are extensively discussed in [20].

There are two processes that necessitate proper accounting of the triplet population. First, because of STA having a direct effect on the optical gain. Secondly, triplets can be excited to higher states by absorption of the light emitted by the singlets, therefore introducing additional optical loss in the cavity. This is referred to as triplet absorption (TA). Triplets are annihilated in the bi-molecular processes of triplet-triplet annihilation (TTA) and triplet-polaron annihilation (TPA). TPA leads to a loss of the triplet, just as SPA for the singlet does. In the next section, we will formulate rate equations for the relevant densities where each of the above-mentioned absorption processes corresponds to a term with corresponding rate coefficient.

The measurements have been performed for an OLED with size 100 μm × 100 μm and Alq3 as the emitting organic molecule. The high-speed OLED device has been deposited on a CPW electrode inspired from the microwave techniques as in [11]. These electrodes and the built-in measurement resistance are patterned by inductively coupled plasma (ICP) technique etching on 340 μm thick indium tin oxide (ITO) coated glass substrate. To improve electrical conduction, the etched electrodes are subjected to metallization by vacuum deposition of 1 nm:150 nm of chrome:gold layers and liftoff process in ultrasonic bath of acetone.
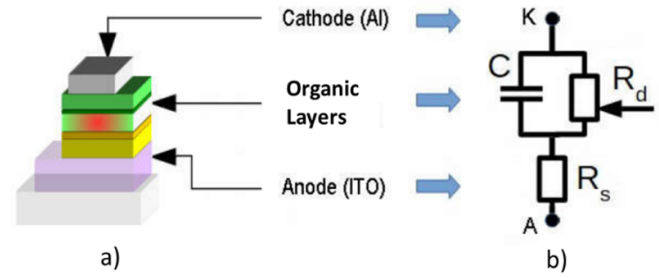
Figure 2. (a) Simplified sketch of the OLED under voltage excitation; (b) equivalent electrical circuit. C is the capacitance, R_d the dynamical ON resistance and R_s the series resistance.

The device consists of 30 nm of 4,4′,4″-tris [(3-methylphenyl)phenylamino] triphenylaminem (MTDATA) as HIL, 10 nm thick N, N′-di (1-naphthyl)-N, N′-diphenyl-(1,1′-biphenyl)-4, 4′-diamine (NPD) as HTL, 30 nm of Alq3 as light EL, 5 nm of 2,2′,2″-(1,3,5-benzinetriyl)-tris(1-phenyl-1-H-benzimidazole (TPBi) as HBL, 25 nm of Alq3 as electron transporting layer, and a final cathode layer of lithium fluoride (LiF) (1 nm)/Al (120 nm). This structure is deposited by vacuum thermal evaporation.

3. Description of the model

3.1. Electrical model

When applying nanosecond electrical pulses, it is essential to consider impedance-matching related effects such as charge loading times and related transients. We will consider the situation where a voltage square pulse of magnitude V_E is applied between the cathode K and the anode A of the OLED (figure 2(a)) during a time interval T. This is the ON-OFF excitation model analyzed by Chime *et al* [11]. They show that the corresponding equivalent electrical model, sketched in figure 2(b), leads to the following expression for the electrical current I_D through the diode:

$$I_D(t) = 0, \qquad \text{for } t < 0;$$
$$I_D(t) = \frac{V_E}{R_d + R_s}\left[1 - \exp\left(-\frac{t}{\tau}\right)\right], \qquad \text{for } 0 < t < T;$$
$$I_D(t) = \frac{V_E}{R_d + R_s}\left[\exp\left(\frac{T}{\tau}\right) - 1\right]\exp\left(-\frac{t}{\tau}\right), \text{ for } t > T. \quad (1)$$

Here, the time constant τ is the electrical response time of the device, given by

$$\tau \equiv \frac{R_d R_s}{R_d + R_s} C, \qquad (2)$$

where the dynamical ON resistance R_d, the series resistance R_s and the capacitance C are indicated in figure 2(b). According to equation (1), the current flow through the diode shows an exponential switch on to its steady value and an exponential switch off, both set by the response time.

Table 1. Model parameters (Alq3).

Symbol	Name	Value	References
A	OLED active area	10^{-4} cm^2	
d	OLED active layer thickness	30 nm	
N_{MOL}	Molecular density	1×10^{-20} cm^{-3}	
γ_0	Zero-field Langevin recombination rate	6.2×10^{-12} cm^3 s^{-1}	[21, 22]
κ_S	Singlet-exciton decay rate	8.0×10^7 s^{-1}	[23]
κ_T	Triplet decay rate	6.5×10^4 s^{-1}	[24]
κ_{ISC}	Inter-system crossing rate	2.2×10^7 s^{-1}	[20]
κ_{SS}	Singlet-singlet annihilation (SSA) rate	3.5×10^{-12} cm^3 s^{-1}	[23]
κ_{SP}	Singlet-polaron annihilation (SPA) rate	9.0×10^{-10} s^{-1}	[23]
κ_{TP}	Triplet-polaron annihilation (TPA) rate	2.8×10^{-13} cm^3 s^{-1}	[23]
κ_{ST}	Singlet-triplet annihilation (STA) rate	5.7×10^{-10} cm^3 s^{-1}	[20, 23]
κ_{TT}	Triplet-triplet annihilation (TTA) rate	2.2×10^{-12} cm^3 s^{-1}	[23]
Γ	Confinement factor	0.29	
ξ_E	Stimulated emission gain coefficient	1.4×10^{-5} cm^3 s^{-1}	[20, 21]
ξ_A	Reabsorption coefficient	1.4×10^{-5} cm^3 s^{-1}	
ξ_{TA}	Triplet absorption (TA) coefficient	1×10^{-7} cm^3 s^{-1}	[25]
κ_{cav}	Cavity photon decay rate	$1–300 \times 10^{12}$ s^{-1}	
β_{sP}	Spontaneous emission factor	<0.15	
V_0	Reference voltage (Poole–Frenkel)	To be determined	Equation (8)
R_d	Dynamical 'on' resistance	70 Ω	Equation (2)
R_s	Series resistance	15 Ω	Equation (2)
C	Capacitance	5 pF	Equation (2)

3.2. ODL rate equations

As mentioned in section 2, the hole-type and electron-type polarons recombine in the EL to form singlet and triplet excitons. We consider the situation where the EL is composed of Alq3 molecules, for which the singlets have their optical emission in the green part of the spectrum peaked around 530 nm and the (Stokes shifted) absorption in the blue part (peaked around 400 nm). In a lumped-cavity model description it is assumed that all densities, including the photons, can be situated in one representative point in the EL. Thus, the equations governing the time evolution of the relevant densities are

$$\frac{\mathrm{d}}{\mathrm{d}t}N_P = \frac{I_D P_0}{eAd} - \gamma N_P^2; \tag{3}$$

$$\begin{aligned}
\frac{\mathrm{d}}{\mathrm{d}t}N_S = {} & \frac{1}{4}\gamma N_P^2 + \frac{1}{4}\kappa_{TT}N_T^2 - (\kappa_S + \kappa_{ISC})N_S \\
& - \left(\frac{7}{4}\kappa_{SS}N_S + \kappa_{SP}N_P + \kappa_{ST}N_T\right)N_S \\
& - \xi_E M_E (N_S - W_0 N_0) N_{PHO};
\end{aligned} \tag{4}$$

$$\begin{aligned}
\frac{\mathrm{d}}{\mathrm{d}t}N_T = {} & \frac{3}{4}\gamma N_P^2 + \kappa_{ISC}N_S + \frac{3}{4}\kappa_{SS}N_S^2 - (\kappa_T + \kappa_{TP}N_P)N_T \\
& - \frac{5}{4}\kappa_{TT}N_T^2 - \xi_E M_E W_T N_T N_{PHO};
\end{aligned} \tag{5}$$

$$\begin{aligned}
\frac{\mathrm{d}}{\mathrm{d}t}N_{PHO} = {} & (\Gamma \xi_E M_E (N_S - W_0 N_0 - W_T N_T) - \kappa_{CAV}) N_{PHO} \\
& + \beta_{sp}\kappa_S N_S;
\end{aligned} \tag{6}$$

$$N_0 = N_{MOL} - 2N_P - N_S - N_T; \quad P_0 = \frac{N_0}{N_{MOL}}. \tag{7}$$

These equations are valid in the EL and the time-dependent variables are: γ the Langevin recombination rate, N_P the polaron density, N_S the density of singlet excitons, N_T the density of triplet excitons, N_0 the density of ground-state molecules, N_{PHO} the photon density, W_0 the reabsorbtion factor and W_T the TA factor. The various parameters in equations (1)–(7) are listed in table 1 together with their values. The rate equations (3)–(6) are extensively discussed by us in [19] and this will not be repeated here. The variables γ, M, W_0 and W_T are time-dependent and need further explanation.

The recombination rate γ in equation (3) is related to the polaron mobilities μ_h and μ_e as $\gamma = \frac{e}{\in}(\mu_h + \mu_e)$. According to the Poole–Frenkel model, the mobilities show exponential dependencies on the square root of the electric field $F = V_D(t)/d$ [26, 27]. In our model we will take

$$\gamma(t) = \gamma_0 e^{\sqrt{V_D(t)/V_0}}, \tag{8}$$

with V_0 an adjustable parameter to be determined in the validation of the model (see section 4) and $V_D(t) = R_d I_D(t)$.

The reabsorption factor W_0 is introduced in [13, 19] and given by

$$W_0 \equiv \frac{\xi_A M_A}{\xi_E M_E}, \tag{9}$$

and the TA factor W_T is defined similarly as

$$W_T \equiv \frac{\xi_{TA} M_{TA}}{\xi_E M_E}, \tag{10}$$

with M defined as

$$M_x \equiv \frac{\int d\lambda S_x(\lambda) S_E(\lambda) S_{CAV}(\lambda)}{\int d\lambda S_E(\lambda) S_{CAV}(\lambda)}, (x = E, A, TA), \quad (11)$$

where $S_E(\lambda)$, $S_A(\lambda)$ and $S_{TA}(\lambda)$ are the emission, reabsorption and triplet absorption spectra, respectively, of the organic material and $S_{CAV}(\lambda)$ is the (Lorentzian) cavity spectrum normalized as $\int d\lambda S_{CAV}(\lambda) = 1$. The spectra S_E, S_A and S_{TA} should be normalized such that $S_x(\lambda_x) = 1$, with λ_x the wavelength for which S_x is maximal ($x = E, A, TA$). In case of a narrow cavity-resonance at wavelength λ_{CAV}, we have $M_x \approx S_x(\lambda_{CAV})$.

The terms for stimulated and spontaneous emission in equation (6) are consistent with those in [25] and [28]. It should be noted that both the cross section for TA in Alq3 and the corresponding absorption spectrum are not very well known. Therefore, and to keep calculations simple, W_T will be approximated in the simulations based on equations (1)–(7) by the time-independent and reasonable value $W_T \sim 0.007$ that can be derived from a TA cross-section value of $\sim 10^{-17}$ cm^2 suggested in [25].

3.3. Brief discussion of the equations, reabsorbtion and emission linewidth

The fraction P_0 in the first term of equation (3) guarantees that polarons can only be created so long molecules in their ground state are available. The second term describes loss of polarons due to the Langevin recombination, where the recombination rate is given by equation (8).

Equation (4) is the balance equation for the creation and annihilation of the singlet excitons, where the last term on the right-hand side (rhs) accounts for the net loss due to stimulated emission. The singlet density provides the optical gain. The evolution of triplet excitons is given by equation (5). Since the triplets suffer relatively small losses, their number can increase substantially. This will hamper the build-up of singlets due to the bi-molecular STA process and suppress the photon density due to TA.

The production of photons in the cavity is described by equation (6), where the first term on the rhs is the net-stimulated emission rate and the second term the rate contribution due to spontaneous emission. The singlet density, for which the net photon loss rate, $\Gamma \xi_E M_E (W_0 N_0 + W_T N_T) + \kappa_{CAV}$, is precisely compensated by the photon stimulated emission rate, defines the threshold for lasing, i.e.

$$N_S|_{thr} = W_0 N_0 + W_T N_T + \frac{\kappa_{CAV}}{\Gamma \xi_E M_E}. \quad (12)$$

We will see in section 5, that laser operation is characterized by clamping of the singlet density very close to the value defined in equation (12).

If we relate, following [29], the frequency linewidth $\Delta\nu$ of the emitted light to the effective photon cavity decay rate (see the first term in equation (6)),

$$\kappa_{CAV,eff} = \kappa_{CAV} + \Gamma \xi_E M_E (W_0 N_0 + W_T N_T - N_S), \quad (13)$$

we obtain

$$\Delta\nu = \frac{\kappa_{CAV,eff}}{2\pi}. \quad (14)$$

This is valid so long the system is quasi-CW and no linewidth enhancement due to amplitude-phase coupling occurs. The cavity width Δ_{CAV} that should be substituted in M_E, W_0 and W_T (see equations (9)–(11)), is related to the linewidth (equation (14)) as $\Delta_{CAV} = \frac{\lambda_E^2}{2\pi c} \Delta\nu$, with c the vacuum light velocity.

The simulations have been performed using analytic expressions for the spectra $S_E(\lambda)$, $S_A(\lambda)$ and $S_{CAV}(\lambda)$ as described in the appendix of [13].

3.4. Simulations below laser threshold

The first simulation results are presented in figure 3 for an OLED *without* a special optical cavity, for which we assume $\kappa_{CAV} \cong 1.3 \times 10^{14}$ s^{-1}, corresponding to $Q \cong 18$. The applied voltage current V_E is switched on at time 0, increases linearly with time during 300 ns to 100 V and then abruptly switched off at $t = 300$ ns. The parameters are as in table 1, except for some values mentioned in the caption of figure 3. In figure 3(a), apart from the current density J_D (blue curve) and the diode voltage V_D (green), time evolutions are seen for the ground-state probability P_0 (red), the reabsorption factor W_0 (orange) and the linewidth $\Delta\nu$ (violet) of the light emitted by the singlet excitons. W_0 and $\Delta\nu$ remain nearly constant at respective values 6.7×10^{-3} and 2×10^{13} s^{-1}. Due to the formation of excitons, the fraction P_0 of molecules in the ground state falls to 0.41, when the total number of excitons approaches 50% of the total number of molecules as can be seen in figure 3(b). At $t = 300$ ns, there are 450 times as many triplets than singlets, i.e. much more than the spin-related factor 3 in the Langevin recombination. This is predominantly due to STA and SSA hampering the growth of singlet excitons. Note in figure 3(b) that the photon density N_{PHO} (red) exhibits the same time development as N_S (blue), apart from a proportionality factor, indicating that stimulated emission is negligibly small.

The maximal singlet density of $\cong 1.1 \times 10^{17}$ cm^{-3} is obtained for $V_E = 100$ V at $t = 300$ ns and this is only 0.3% of the value needed for laser operation. As it is not feasible to apply much larger voltages without damaging the device, the only possibility to attain laser threshold is by lowering $N_S|_{thr}$. As can be seen from equation (12), one way to realize this is by lowering κ_{CAV}, which is equivalent to increasing the quality factor of the cavity. Also keeping reabsorption, i.e. W_0, P_0 and TA i.e. W_T, small will help in this respect. This will be investigated in section 5.

The situation studied so far is for slowly increasing applied voltage which is slow on the system's shortest dynamical timescale of ~ 10 ns and resembles a situation of quasi-CW excitation. The situation of short pulses ≤ 2 ns requires special attention since the underlying polaronic and excitonic dynamics behave quite differently. Figure 4 shows an overview of the time evolutions of the relevant variables after pulse excitation of voltage $V_E = 20$ V from $t = 0$ to $t = 2$ ns, whereafter the voltage drops abruptly to 0. In figure 4(b) we observe that the maximal singlet density N_S at $t = 2$ ns is a factor 430 smaller
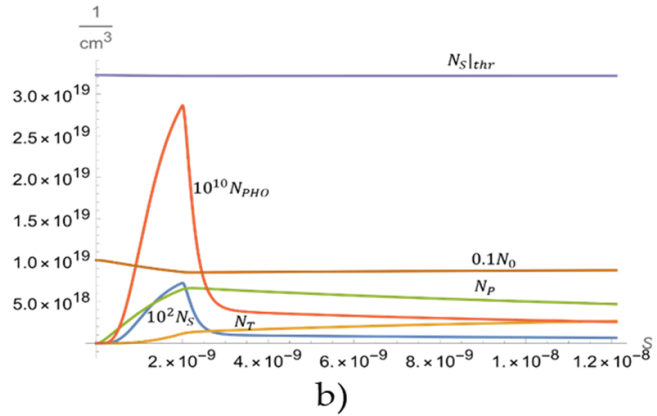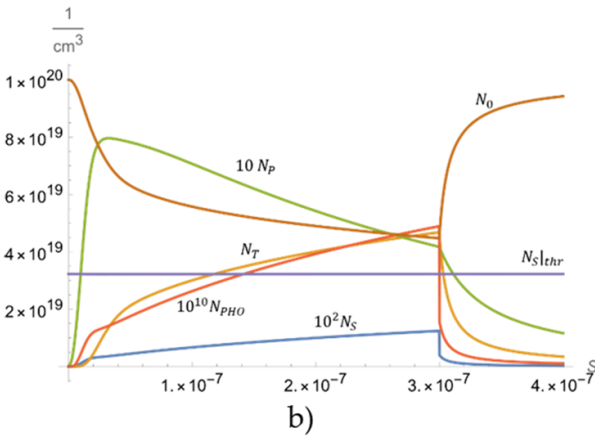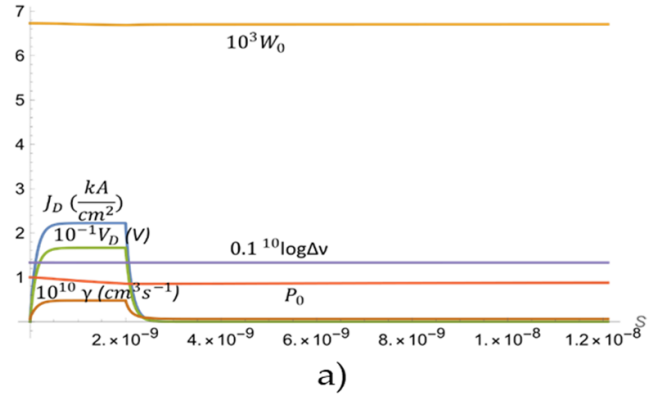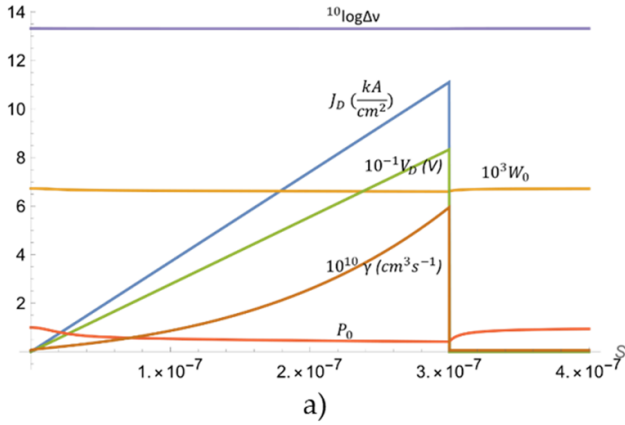
Figure 3. Overview of the time evolution of the relevant variables after linear increase of the excitation voltage V_E from 0 at $t = 0$–100 V at $t = 300$ ns, whereafter the voltage drops abruptly to 0. In (a) the diode current density J_D is seen to increase linearly from 0 to 11.1 kA cm^{-3} and the diode voltage V_D from 0 to 84 V. In (b) we observe that the maximal singlet density N_S at $t = 300$ nm is still a factor 290 smaller than the laser threshold value. The photon emission is predominantly by spontaneous emission. $\kappa_{CAV} = 1.28 \times 10^{14}$ s^{-1}, $\beta_{sp} = 0.064$, $V_0 = 4$ V and other parameters as in table 1.

Figure 4. Overview of the time evolution of the relevant variables after pulse excitation of voltage $V_E = 20$ V from $t = 0$ to $t = 2$ ns, whereafter the voltage drops abruptly to 0. In (a) the diode current density J_D is seen to quickly increase to a value of 2.2 kA cm^{-3} and the diode voltage V_D to 16.6 V. In (b) we observe that the maximal singlet density N_S at $t = 2$ ns is a factor 450 smaller than the laser threshold value. The photon emission is predominantly by spontaneous emission. The optical response has a peak width of 1.2 ns and shows a very slowly decaying long tail, governed by the slow decay of the polarons. $\kappa_{CAV} = 1.28 \times 10^{14}$ s^{-1}, $\beta_{sp} = 0.064$, $V_0 = 4$ V and other parameters as in table 1.

than the laser threshold value. The photon emission is predominantly by spontaneous emission and shows a narrow peak of width 1.2 ns followed by a slowly decaying long tail. This tail is due to the slow decay of the polarons N_P (green, decay time ~40 ns).

4. Short-pulse measurements and calibration of the model

4.1. Short-pulse measurements

The measurements have been performed for an OLED with size 100 μm $\times$ 100 μm and Alq3 as the emitting organic molecule. The high-speed OLED device has been deposited on a CPW electrodes inspired from the microwave techniques as in [11]. These electrodes and the built-in measurement resistance are patterned by ICP etching on 340 μm thick ITO coated glass substrate. To improve electrical conduction, the etched

electrodes are subjected to metallization by vacuum deposition of 1 nm:150 nm of chrome:gold layers and liftoff process in ultrasonic bath of acetone. The external quantum efficiency of the device is estimated 0.004 at the applied voltage of 22 V. This value follows from our simulation and agrees well with experimental values reported in [30].

The measurement system, consisting of a probe station (Cascade PM5), a high speed pulse generator (AVTECH AVP AVHV3-B), a digital oscilloscope (Tektronix TDS 6604), and a photodiode with 400 MHz bandwidth (Thorlabs APD430 A2), enables a simultaneous single shot measurement of the device current density and light emission while the device is submitted to electrical pulses with pulse width ranging from 400 ps to 1 ns. All measurements are realized in ambient atmosphere at room temperature.

Single-shot measurements of the voltage excitation signal, electrical response, and optical response are shown in figure 5. Clear optical response is detected for electrical pulse widths of
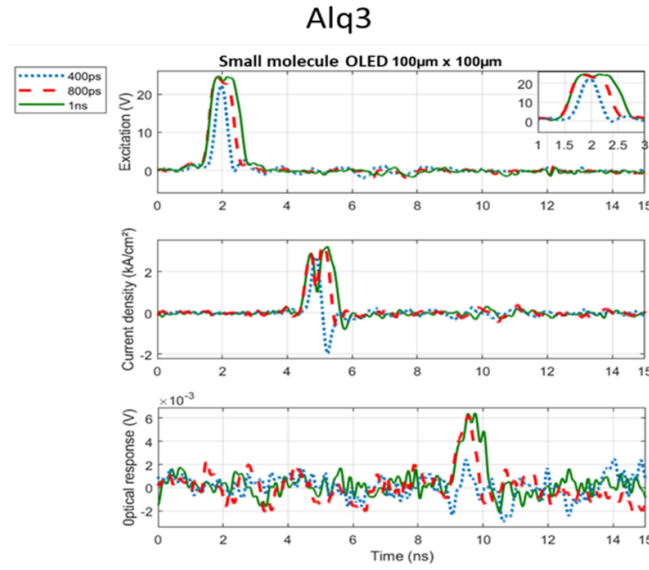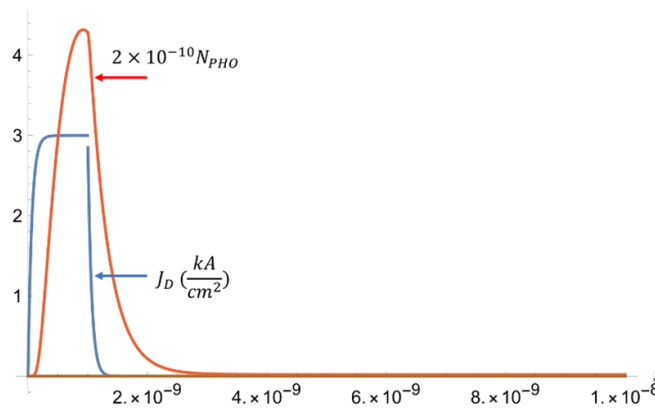
Figure 5. Applied voltage (upper window), measured current density (middle window), and observed photon power (lower window) for pulse durations of 0.4 ns (blue), 0.8 ns (red) and 1.0 ns (green).

Table 2. Calibration criteria derived from the measurements.

Nominal width (ns)	Current density maximum (kA cm^{-2})	Current density pulse duration FWHM (ns)	Optical response maximum (AU)	Optical response pulse duration FWHM (ns)
0.4	2.5	0.35	0.6	0.35
0.8	3.0	0.85	1.35	0.7
1.0	3.0	1.0	1.40	1.0

Figure 6. Simulation for $V_0 = 0.4$ V of the time evolution of the relevant variables after pulse excitation during 1 ns of voltage $V_E = 25.5$ V, whereafter the voltage drops abruptly to 0. The diode current density J_D is seen to quickly increase to a value of 3.0 kA cm^{-2} and falls rapidly to zero after 1 ns. The optical response has a peak width of 0.8 ns and shows a rapidly decaying tail, as in the measurement of figure 5. $\kappa_{CAV} = 1.16 \times 10^{15}\,s^{-1}$, $\beta_{sp} = 0.58$ and other parameters as in table 1.

Table 3. Simulated ($V_0 = 0.4$ V) and observed optical response data for the measurements of figure 5.

Nominal width (ns)	Simulated width (FWHM, ns)	Simulated height (AU)	Simulated height (relative)	Measured width (FWHM, ns)	Measured height (relative)
0.4	0.5	1.6	0.36	0.4	0.45
0.8	0.7	4.3	0.98	0.7	0.95
1.0	0.8	4.4	1.0	1.0	1.0

0.4, 0.8 and 1.0 ns. In all cases, the applied voltage amplitude was set at 22 V. For pulses shorter than 0.4 ns, no significant optical responses were observable. Note that the widths of the optical response pulses are roughly equal to the electrical pulse width, but the height ratios of current density and optical power differ. These data will be used to calibrate our theory.

### 4.2. Validation of the model for short pulse excitation below threshold

The criteria derived from figure 5 that will be used to calibrate our theory are (a) the top level of the observed electrical current density, (b) the relative top value and (c) the full width at half maximum (FWHM) of the optical response pulse. These values are given in table 2. One important adjustment parameter in the simulation is V_0 (see equation (8)). It regulates the value of the Langevin recombination rate γ during the exciting pulse and therefore has a strong effect on the width of the optical response pulse. The smaller V_0, the larger γ becomes, whereas large V_0 leads to slow decay of the tail. In the appendix we compare photon response pulse shapes for four different values of V_0 and nanosecond excitation at $J_D = \frac{I_D}{A} \sim 3\,\text{kA cm}^{-2}$.

The best V_0 value for which the measured pulses could be reproduced is $V_0 = 0.4\,\text{V}\,(\pm 10\%)$, with all other parameter values as in table 1. Figure 6 shows a simulation for this value of V_0 for an excited pulse of 3 kA cm^{-2} during 1 ns. For this case we find a FWHM of 0.8 ns. Table 3 summarizes the findings for the three cases of figure 5.

5. Above laser threshold

We will now repeat the simulation as in figure 3 but for a high-Q cavity with $Q = 6000$ and all other parameters as in table 1. The result presented in figure 7 convincingly shows that no laser operation will take place, no matter how long we continue electrical excitation. However, with a step excitation we do find a threshold current at $\sim 0.75\,\text{kA cm}^{-2}$, above which the system responds with a short ns laser pulse, followed by GHz relaxation oscillations. This is illustrated in figure 8, which shows the time evolution of the various variables after switch-on of a constant current density $J_D \cong 4.6\,\text{kA cm}^{-2}$. The duration of the laser response pulse is ~ 3 ns, but decreases monotonously when decreasing the current density to the threshold value for pulsed response ($\sim 0.75\,\text{kA cm}^{-2}$).

Since a quality factor of 6000 is rather difficult to realize in the above-described micro OLEDS, we investigated numerically how requirements on the quality factor can be released. This has resulted in the combinations of parameters that yield laser threshold conditions depicted in tables 4 and 5. These results predict feasible conditions for pulsed laser operation. It should be noted that a nanosecond pulsed current density of up to 60 kA cm^{-2} is feasible in our LPL laboratory in Paris.
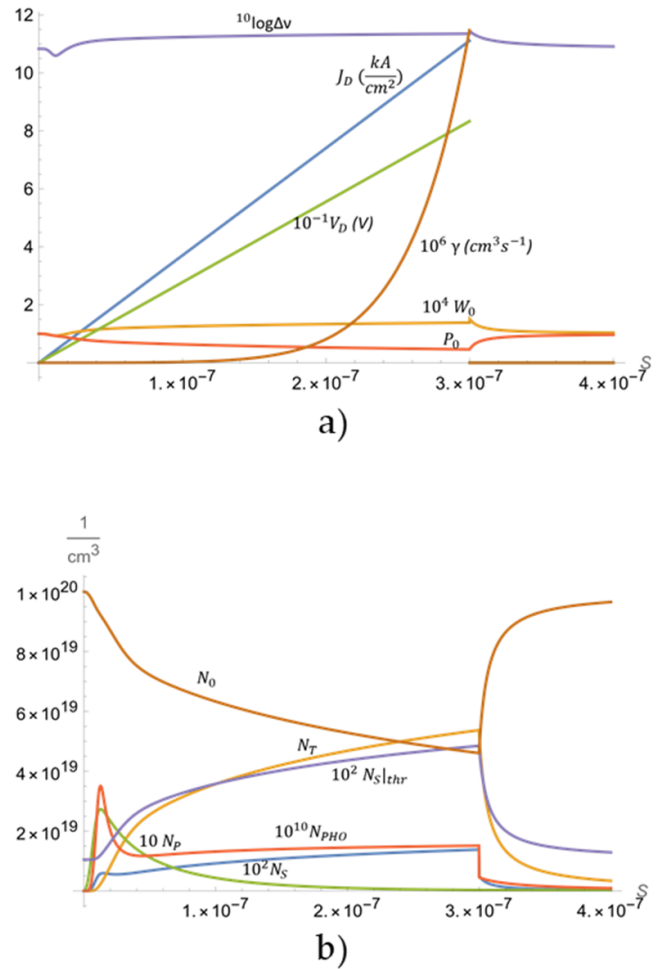

Figure 7. Same as figure 3, except $q = 6000$ ($\kappa_{\text{CAV}} = 3.85 \times 10^{11}\,\text{s}^{-1}$), $\beta_{\text{sp}} = 0.000\,193$ and $V_0 = 0.4$ V. No threshold for lasing is reached. In (a) we observe that due to the narrow cavity spectrum, the reabsorption fraction W_0 is a factor 70 smaller than in figure 3 and that the effective linewidth increases, except for the first ~ 10 ns. This is due to TA increasing the gap between N_S and $N_S|_{\text{thr}}$ as can be seen in (b). Other parameters as in table 1.

6. Threshold predictions for nanosecond pulsed lasing

6.1. Analytical

In the previous section we obtained some threshold predictions for the combination of parameters given in table 1 and the value $V_0 = 0.4$ V, following from the fit of the theory to the measurements far below threshold. In the present section we will derive an analytical estimate for the threshold condition for pulsed lasing and investigate which parameters prospective gain materials should possess if they were to lead to feasible lasing conditions. These findings will be backed up by numerical simulations.

The complex dynamics described by equations (3)–(7) allow an approximate analytic solution in case of short-pulse excitation. In this regime, N_S and N_P will assume their maximum value after a few ns and these values can be
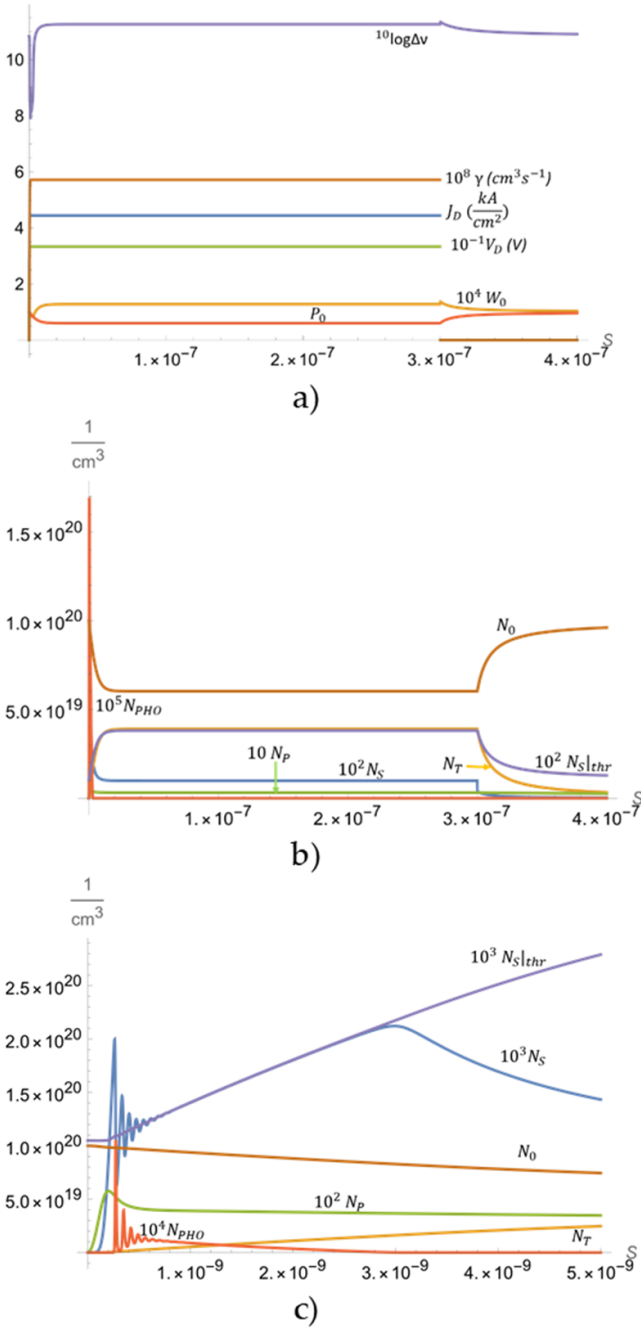
Figure 8. Same as figure 7, except with a DC electrical current, switched on at $t = 0$ and off at $t = 300$ ns and in (c) a zoom-in of the first 5 ns. The current density is $J_D \cong 4.6$ kA cm^{-2}. The damped relaxation oscillation of ~ 14 GHz is clearly seen in (c) as well as the clamping of N_S to its threshold value $N_S|_{thr}$ up to ~ 3 ns.

found from equations (3) and (4) by equating the right-hand sides to zero, yielding

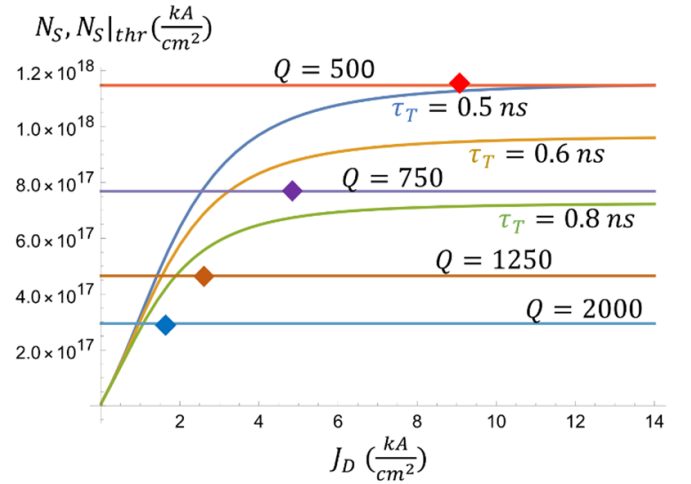$$N_P \sim \sqrt{\frac{I_D}{eAd\gamma}} = \sqrt{\frac{J_D}{ed\gamma}}, \tag{15}$$

$$N_S \sim \frac{\dfrac{J_D}{4ed}}{\kappa_S + \kappa_{ISC} + \kappa_{SP}N_P + \kappa_{ST}N_T} \tag{16}$$

Table 4. Parameter combinations for pulsed laser threshold at fixed current density equal to 10 kA cm^{-2}.

V_0 (V)	0.4	1.0	2.5
Q	480	540	850

Table 5. Parameter combinations for pulsed laser threshold at fixed $Q = 1000$.

V_0 (V)	0.4	1.0	2.5
J_{thr} (kA cm^{-2})	3.2	5.1	8.7

Figure 9. N_S curves given by equation (16) for three values of τ_T as indicated. Other parameters are for Alq3 (table 1 and $V_0 = 0.4$ V). The horizontal lines are the short-pulse lasing threshold values for N_S at the three indicated Q-values. The diamonds show the threshold current densities at the corresponding Q obtained from full simulations.

where $J_D = I_D/A$ is the current density and where we should substitute an educated guess for the value of N_T. For this we integrate the first term in the right hand side of equation (5) from $t = 0$ to the time τ_T at which the maximum of N_S is attained, yielding

$$N_T \sim \frac{3}{4}\left(\gamma N_P^2 \tau_T - N_P\right). \tag{17}$$

We have assumed that for these short times $P_0 \cong 1$.

Numerical evaluation of equations (15)–(17) using equation (8), shows that the result (equation (15)) for N_S strongly depends on τ_T. Figure 9 presents N_S from equation (16) versus the applied current density for $\tau_T = 0.3, 0.4$ and 0.5 ns. The horizontal lines indicate the threshold values $N_S|_{thr}$ for lasing (see equation (12)) for quality factors $Q = 500, 750, 1250$ and 2000, and other parameters as in figure 6. The diamonds indicate the values obtained from the full simulations. There is reasonable agreement. An overview of numerically obtained threshold values for various different Q-factors is given in table 6.

According to equation (16), the most important parameters that determine the pulsed lasing threshold are κ_S, κ_{ISC},

Table 6. Predicted nanosecond pulsed laser threshold currents for Alq3 under step excitation.

Q	$J_D|_{thr}$ (kA cm^{-2})
250	48
500	9.4
750	4.7
1000	3.2
2500	1.4
5000	0.85
6000	0.75
8000	0.62
10 000	0.53
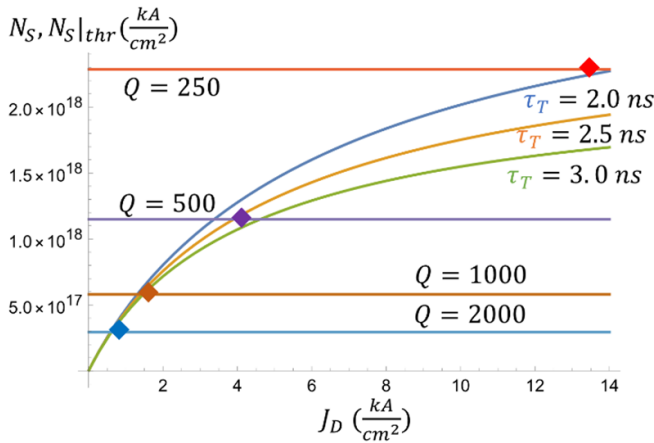
Figure 10. N_S curves given by equation (16) for three values of τ_T as indicated. Parameters are $\kappa_S = 1 \times 10^9$ s^{-1}, $\kappa_{ST} = 5 \times 10^{-11}$ cm^3 s^{-1}, $\kappa_{SP} = 1 \times 10^{-11}$ cm^3 s^{-1}, $V_0 = 0.4$ V and other parameters as in table 1. The horizontal lines are the short-pulse lasing threshold values for N_S at the four indicated Q-values. The diamonds show the threshold current densities at the corresponding Q obtained from full simulations.

κ_{SP} and κ_{ST}. Hence, when identifying an active organic molecule with the lowest injection current density, we should go for small values for these parameters. In this respect, a large value for γ will help as well, since it leads to small N_P. To illustrate this, figure 10 depicts the results in case of parameters $\kappa_S = 10^9$ s^{-1}, $\kappa_{ST} = 5 \times 10^{-11}$ cm^3 s^{-1}, $\kappa_{SP} = 1 \times 10^{-11}$ cm^3 s^{-1}, $V_0 = 0.4$ V and other parameters as in table 1. The colored diamonds in figure 10 correspond to the threshold current densities at the corresponding Q obtained from full simulations.

6.2. Numerical

To investigate DC operation we rely on full simulations for estimations of laser thresholds. It turns out that for DC excitation the saturation value of N_T becomes so large that the build-up of singlets is seriously hampered (gain quenching) and the photon density suffers from absorption by triplets (TA). The singlet build-up is mostly determined by the value of the STA parameter κ_{ST} and also by the SPA parameter κ_{SP}. In this respect, the value of the Poole–Frenkel parameter V_0 is crucial. For small values $V_0 \leq 1$, the steady-state value for N_P remains

small and SPA is of minor importance for the lasing threshold. The opposite is true when $V_0 \gg 1$. In this case the polaron density becomes high and SPA important.

As the value of V_0 is not a very well-known material property, it is difficult to make generic realistic predictions for the CW-laser threshold. For the special case of Alq3 as gain material, we did not find CW-lasing even for high-quality cavities. In fact, for the value of $\xi_{TA} = 1 \times 10^{-7}$ cm^3 s^{-1} as in table 1, the gap between N_S and $N_S|_{thr}$ increases for increasing current. This critically depends on the actual value for ξ_{TA}. For $\xi_{TA} = 1 \times 10^{-8}$ cm^3 s^{-1} the simulation does yield a threshold current for CW-lasing with a high-Q cavity ($Q = 6000$) of $J_D|_{thr} = 10.7$ kA cm^{-2}. This would correspond to a rather small, if not unrealistic, cross section $\sigma_{TA} \approx 5 \times 10^{-19}$ cm^2.

In general, small values for κ_{ST}, κ_{SP} and ξ_{TA} combined with large Q values are helpful for achieving small laser threshold currents. The former three parameters are characteristic properties of the emitting material, whereas the latter can be controlled, in principle, by proper cavity design and engineering.

Assuming smaller values for κ_{ST} and κ_{SP} than in table 1, i.e. $\kappa_{ST} = 1 \times 10^{-12}$ cm^3 s^{-1}, $\kappa_{SP} = 1 \times 10^{-11}$ cm^3 s^{-1}, $\xi_E = \xi_A = 6.4 \times 10^{-6}$ cm^3 s^{-1}, $\kappa_{ISC} = 2.2 \times 10^4$ s^{-1}, $V_0 = 0.4$ V and other parameters as in table 1, we find CW laser operation with a linewidth of ~ 5 GHz in a simulation longer than 1000 ns electrical pumping with $J_D \cong 1.1$ kA cm^{-2} and $Q = 500$. For this case, a laser threshold for CW operation is predicted at $\cong 0.66$ kA cm^{-2}. These parameter values might apply to the organic material BsB-Cz [19, 20].

7. Discussion and conclusions

We have applied our improved organic-laser theory to sub-nanosecond pulsed electrical excitation of a micro OLED with the organic material Alq3 (aluminum tris(8-hydroxyquinoline)) as light-EL. We obtained a best fit value for the Poole–Frenkel threshold parameter V_0 that plays an essential role in the polaronic Langevin recombination. Simulations on the basis of our theory show that due to the accumulation of triplet excitons gain quenching occurs after a few nanoseconds. As a result of this, pulsed laser operation during the first few nanoseconds is much easier to achieve than DC operation. Using the above-mentioned fit for V_0, we predict threshold current densities in case of Alq3 as gain material for short-pulse lasing. For Q values >500, threshold currents for short-pulse lasing are found to be <9.4 kA cm^{-2}, which are feasible current densities. On the other hand, we did not find CW laser operation for Alq3, but for organic materials with one or two orders of magnitude smaller STA, SPA and/or TA, CW laser operation for feasible current densities and Q-factors, may very well be possible.

Data availability statement

The data that support the findings of this study are available upon reasonable request from the authors.
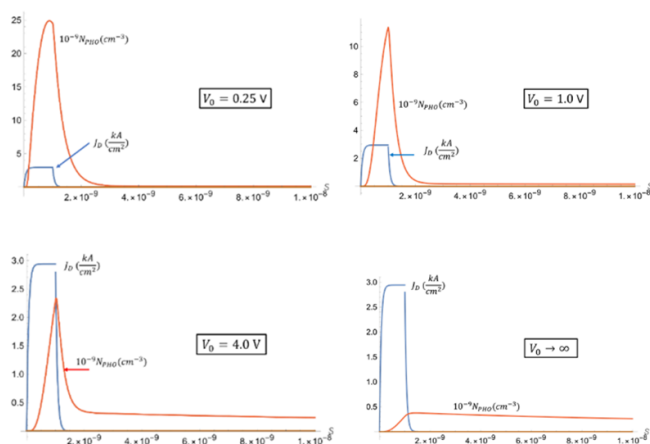
Figure 11. Effect of V_0 on the shape of the optical response. For large V_0 the response pulse develops a slowly decaying tail, causing the response to last much longer than the exciting pulse (here 1 ns in each case). Note the equal height of the electrical pulse in all cases. Parameters as in table 1 and $Q = 18$.

Acknowledgments

Appendix. Influence of V_0

In figure 11 photon response pulses are shown for four values of V_0 as indicated, and for each case the same electrical exciting pulse of 1 ns.

ORCID iDs

Daan Lenstra https://orcid.org/0000-0002-4000-8897
Alexis P A Fischer https://orcid.org/0000-0001-8534-6905
Alex Chamberlain Chime https://orcid.org/0000-0002-2670-6808

References

[1] Islim M S *et al* 2017 Towards 10Gb/s orthogonal frequency division multiplexing based visible light communication using a GaN violet micro-LED *Photon. Res.* **5** A35–A43
[2] Yoshida K, Manousiadis P P, Bian R, Chen Z, Murawski C, Gather M C, Haas H, Turnbull G A and Samuel I D W 2020 245 MHz bandwidth organic light-emitting diodes used in a gigabit optical wireless data link *Nat. Commun.* **11** 1171
[3] Yang Y, Turnbull G A and Samuel D W 2010 Sensitive explosivevapor detection with polyfluorene lasers *Adv. Funct. Mater.* **20** 2093–7
[4] Chiang C K, Fincher J C R, Park Y W, Heeger A J, Shirakawa H, Louis E J, Gau S C G and MacDiarmid A 1977 Electrical conductivity in doped polyacetylene *Phys. Rev. Lett.* **39** 1098–101
[5] Fitzner R *et al* 2012 Correlation of π-conjugated oligomer structure with film morphology and organic solar cell performance *J. Am. Chem. Soc.* **134** 11064–7
[6] Lee K H, Leem D-S, Sul S, Park K-B, Lim S-J, Han H, Kim K-S, Jin Y and Lee S 2013 A high performance green-sensitive organic photodiode comprising a bulk heterojunction of dimethyl-quinacridone and dicyanovinyl terthiophene *J. Mater. Chem.* C **1** 2666
[7] Wang C, Dong H, Hu W, Liu Y and Zhu D 2011 Semiconducting π-conjugated systems in field-effect transistors: a material odyssey of organic electronics *Chem. Rev.* **112** 2208
[8] Han T-H, Lee Y, Choi M-R, Woo S-H, Bae S-H, Hong B H, Ahn J-H and T-w L 2012 Extremely efficient flexible organic light-emitting diodes with modified graphene anode *Nat. Photon.* **6** 105–10
[9] Barlow I A, Kreouzis T and Lidzey D G 2009 High-speed elect-roluminescence modulation of a conjugated-polymer light-emitting diode *Appl. Phys. Lett.* **94** 243301
[10] Haigh P A, Ghassemlooy Z, Rajbhandari S and Papakonst-antinou I 2013 Visible light communications using organic light emitting diodes *IEEE Commun. Mag.* **51** 148–54
[11] Chime A C, Bensmida S, Chakaroun M, Lee M W, Nkwawo H and Fischer A P A 2018 Electrical modelling and design of ultra-fast micro-OLED with coplanar wave-guided electrodes in ON-OFF regime *Org. Electron.* **56** 284–90
[12] Braun D, Moses D, Zhang C and Heeger A J 1992 Nanosecond transient electroluminescence from polymer light-emitting diodes *Appl. Phys. Lett.* **61** 3092
[13] Lenstra D, Fischer A P A, Ouirimi A, Chime A C, Loganathan N and Chakaroun M 2021 Organic diode laser dynamics: rate-equation model, reabsorption, validation and threshold predictions *Photonics* **8** 279
[14] Segura J L 1998 The chemistry of electroluminescent organic materials *Acta Polym.* **49** 319–44
[15] Chenais S and Forget S 2011 Recent advances in solid-state organic lasers *Polym. Int.* **61** 390–406
[16] Gozhyk I 2012 Polarization and gain phenomena in dye-doped polymer micro-lasers *Thesis Ecole Normale Superieure* Cachan, France
[17] Senevirathne C A M, Sandanayaka A S D, Karunathilaka B S B, Fujihara T, Bencheikh F, Qin C, Goushi K, Matsushima T and Adachi C 2021 Markedly improved performance of optically pumped organic lasers with two-dimensional distributed-feedback gratings *ACS Photonics* **8** 1324–34
[18] Sandanayaka A S D, Matsushima T, Bencheikh F, Terakawa S, Potscavage W J Jr, Qin C, Fujihara T, Goushi K, J-c R and Adachi C 2019 Indication of current-injection lasing from an organic semiconductor *Appl. Phys. Express* **12** 061010
[19] Ouirimi A, Chime A C, Loganathan N, Chakaroun M, Fischer A P A and Lenstra D 2021 Threshold estimation of an organic laser diode using a rate-equation model validated experimentally with a microcavity OLED submitted to nanosecond electrical pulses *Org. Electron.* **97** 106190
[20] Gärtner C 2008 Organic laser diodes: modelling and simulation *Thesis Doktor Ingenieurs* Universität Karlsruhe, Germany
[21] Gärtner C, Karnutsch C, Pflumm C and Lemmer U 2007 Numerical device simulation of double-heterostructure

organic laser diodes including current-induced absorption processes *IEEE J. Quantum Electron.* **43** 1006–17

[22] Juhasz P, Nevrela J, Micjan M, Novota M, Uhrik J, Stuchlikova L, Jakabovic J, Harmatha L and Weis M 2016 Charge injection and transport properties of an organic light-emitting diode *Beilstein J. Nanotechnol.* **7** 47–52

[23] Kasemann D, Brückner R, Fröb H and Leo K 2011 Organic light emitting diodes under high currents explored by transient electroluminescence on the nanosecond scale *Phys. Rev.* B **84** 115208

[24] Tsutsumi N and Hinode T 2017 Tunable organic distributed feedback dye laser device excited through Förster mechanism *Appl. Phys.* B **123** 93

[25] Chua S-L, Zhen B, Lee J, Bravo-Abad J, Shapira O and Soljačić M 2014 Modeling of threshold and dynamics behavior of organic nanostructured lasers *J. Mater. Chem.* C **2** 1463–73

[26] Torricelli F and Colalongo L 2009 Unified mobility model for disordered organic semiconductors *IEEE Electron Device Lett.* **30** 1048–50

[27] Murgatroyd P N 1970 Theory of space-charge-limited current enhanced by Frenkel effect *J. Phys. D: Appl. Phys.* **3** 151–6

[28] Giebink N C and Forrest S R 2009 Temporal response of optically pumped organic semiconductor lasers and its implication for reaching threshold under electrical excitation *Phys. Rev.* B **79** 073302

[29] Coldren L A, Corzine S and Mashanovitch M 2012 *Diode Lasers and Photonic Integrated Circuits* 2nd edn (New York: Wiley) p 293

[30] Chime A C Etude théorique et expérimentale de micro-OLEDs rapides sur électrodes coplanaires en régime d'impulsions à haute densité de courant *Thesis University Paris* 13 Paris, France (https://doi.org/10.1057/s41271-020-00273-8)